ATLAS NOTE

ATLAS-CONF-2013-073

July 18, 2013

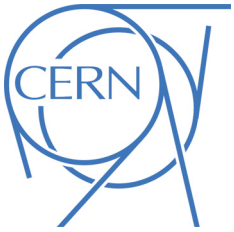

Search for dark matter pair production in events with a hadronically decaying W or Z boson and missing transverse momentum in pp collision data at $\sqrt{s} = 8$ TeV with the ATLAS detector

The ATLAS Collaboration

Abstract

A search is presented for dark matter pair production in association with a W or Z boson in pp collisions corresponding to 20.3 fb^{-1} of integrated luminosity at $\sqrt{s} = 8$ TeV using data recorded with the ATLAS detector at the Large Hadron Collider. Events with large missing transverse momentum and a jet with mass consistent with a W or Z boson decay are analyzed. The data are consistent with the Standard Model expectations, and limits are set on the mass scale in effective field theories which describe the interaction of dark matter and Standard Model particles.

Although the presence of dark matter in the universe is well established, little is known of its particle nature or its non-gravitational interactions. A suite of experiments is searching for a weakly interacting massive particle (WIMP), denoted as χ, and for interactions between χ and Standard Model (SM) particles [1, 2, 3, 4, 5, 6, 7].

One critical component of this program is the search for pair-production of WIMPs at particle colliders, specifically $pp \to \chi\bar{\chi}$ at the Large Hadron Collider (LHC) via some unknown intermediate state. These searches have greatest sensitivity at low m_χ where direct detection experiments are less powerful. At the LHC, the final state WIMPs are invisible to the detectors, but the events can be detected if there is associated initial-state radiation of a SM particle [8]; see an example in Fig. 1.

The LHC collaborations have reported limits on the cross section of $pp \to \chi\bar{\chi} + X$ where X is a hadronic jet [9, 10] or a photon [11, 12]. Other LHC data have been reinterpreted to constrain models where X is a leptonically decaying W [13] or Z boson [14, 15]. In each case, limits are reported in terms of the mass scale M_* of the unknown interaction expressed in an effective field theory as a four-point contact interaction [16, 17, 18, 19, 20, 21, 22, 23, 24]. In the models considered until now, the strongest limits come from mono-jet analyses, due to the large rate of gluon or quark initial-state radiation relative to photon, W- or Z-boson radiation. The operators studied in these mono-jet and mono-photon searches assume equal couplings of the dark matter particles to up-type and down-type quarks ($C(u) = C(d)$). For W-boson radiation there is interference between the diagrams in which the W boson is radiated from the u or the d-quark. In the case of equal coupling the interference is destructive and gives a small W-boson emission rate. If, however, the up-type and down-type couplings have opposite signs ($C(u) = -C(d)$), the relative rates of gluon, photon, Z- or W-boson emission can change dramatically [13], such that mono-W-boson production is the dominant process.

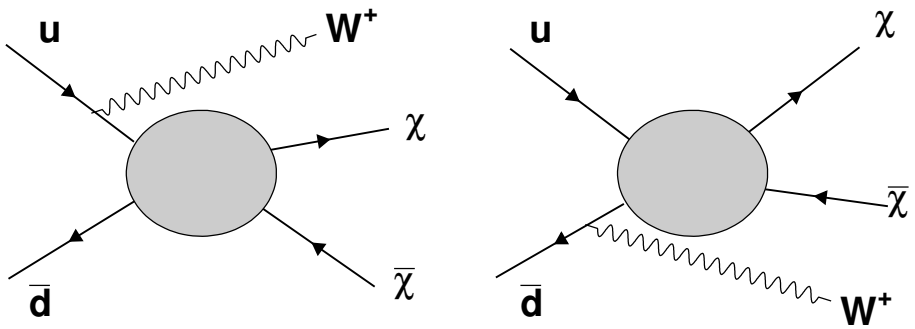

Figure 1: Pair production of WIMPs ($\chi\bar{\chi}$) in proton-proton collisions at the LHC via an unknown intermediate state, with initial-state radiation of a W boson.

In this note, a search is reported for the production of W or Z bosons decaying hadronically (to $q\bar{q}'$ or $q\bar{q}$, respectively) and reconstructed as a single massive jet in association with large missing transverse momentum from the undetected $\chi\bar{\chi}$ particles. This search, the first of its kind, is sensitive to WIMP pair production, as well as other dark-matter-related models, such as invisible Higgs-boson decays (Wh or Zh production with $h \to \chi\bar{\chi}$).

The ATLAS detector [25] at the LHC covers the pseudorapidity [1]range of $|\eta| < 4.9$ and the full azimuthal angle ϕ. It consists of an inner tracking detector surrounded by a thin superconducting solenoid,

[1]ATLAS uses a right-handed coordinate system with its origin at the nominal interaction point (IP) in the center of the detector and the z-axis along the beam pipe. The x-axis points from the IP to the center of the LHC ring, and the y-axis points upward. Polar coordinates (r, ϕ) are used in the transverse (x, y)-plane, ϕ being the azimuthal angle around the beam pipe. The pseudorapidity is defined in terms of the polar angle θ as $\eta = -\ln\tan(\theta/2)$.

electromagnetic and hadronic calorimeters, and an external muon spectrometer incorporating large superconducting toroidal magnets. A three-level trigger system is used to select interesting events for recording and subsequent offline analysis. Only data for which beams were stable and all subsystems described above were operational are used. Applying these requirements to pp collision data, taken at a center-of-mass energy of $\sqrt{s} = 8$ TeV with stable beam conditions during the 2012 LHC run, results in a data sample with a time-integrated luminosity of 20.3 fb^{-1}, determined with an uncertainty of 2.8% following the same methodology as that detailed in [26].

Jet candidates are reconstructed using the Cambridge-Aachen algorithm [27] with a radius parameter of 1.2 to capture the hadronic products of both quarks from W- or Z-boson decay and are referred to as *large-radius jets*. The internal structure of the large-radius jet is probed in terms of the momentum balance of the two leading sub-jets, as $\sqrt{y} = \min(p_{\mathrm{T1}}, p_{\mathrm{T2}})\Delta R/m_{\mathrm{jet}}$ [28, 29] where $\Delta R = \sqrt{\Delta\phi_{1,2}^2 + \Delta\eta_{1,2}^2}$ and m_{jet} is the mass of the jet. In addition, jet candidates are also reconstructed using the anti-k_t clustering algorithm [30] with a radius parameter of 0.4, referred to as *narrow jets*. The inputs to both algorithms are clusters of energy deposits in calorimeter cells seeded by those with energies signicantly above the measured noise and calibrated at the hadronic scale [31]. Jet momenta are calculated by performing a four-vector sum over these cell energy clusters, treating each topological cluster [31] as an $(E, \vec{p})$ four-vector with zero mass. The direction of $\vec{p}$ is given by the line joining the vertex with the energy cluster. Missing transverse momentum, $E_{\mathrm{T}}^{\mathrm{miss}}$, is measured using all clusters of energy deposits in the calorimeter up to $|\eta|$ of 4.5. Electrons, muons, jets and $E_{\mathrm{T}}^{\mathrm{miss}}$ are reconstructed as in Refs. [32, 33, 34, 35] respectively. Reconstruction of hadronic W decays with large-radius jets is validated in a control region with one muon, one large-radius jet ($p_{\mathrm{T}} > 250$ GeV, $|\eta| < 1.2$), two additonal narrow jets ($p_{\mathrm{T}} > 40$ GeV, $|\eta| < 4.5$) separated from the leading large-radius jet, at least one b-tag and $E_{\mathrm{T}}^{\mathrm{miss}} > 250$ GeV, which is dominated by $t\bar{t}$ events (Fig. 2).

Candidate signal events must be accepted by an inclusive $E_{\mathrm{T}}^{\mathrm{miss}}$ trigger which is found to be more than 99% efficient for events with $E_{\mathrm{T}}^{\mathrm{miss}} > 150$ GeV. Events with significant detector noise and non-collision backgrounds are rejected as done in Ref. [9]. In addition, events are required to have at least one large-radius jet with $p_{\mathrm{T}} > 250$ GeV, $|\eta| < 1.2$, mass between 50 and 120 GeV and $\sqrt{y} > 0.4$. Two signal regions are defined by two thresholds in $E_{\mathrm{T}}^{\mathrm{miss}}$, at 350 and 500 GeV. To supress the $t\bar{t}$ background, events are rejected if they contain more than one narrow jet with $p_{\mathrm{T}} > 40$ GeV, $|\eta| < 4.5$ and a separation from the leading large-radius jet of $\Delta R > 0.9$, or if any narrow jet has $\Delta\phi(E_{\mathrm{T}}^{\mathrm{miss}}, \mathrm{jet}) < 0.4$. Finally, to suppress contributions from $W \to \ell\nu$ production, events are rejected if they have any electron candidates with $p_{\mathrm{T}} > 10$ GeV and $|\eta| < 2.47$, photon candidates with $p_{\mathrm{T}} > 10$ GeV and $|\eta| < 2.37$ or muon candidates with $p_{\mathrm{T}} > 10$ GeV and $|\eta| < 2.5$.

The dominant source of background events is $Z \to \nu\bar{\nu}$ production in association with jets from initial-state radiation. A secondary contribution comes from production of jets in association with W bosons with leptonic decays or hadronic τ lepton decay or Z bosons with charged lepton decays in which the charged leptons fail identification requirements. These three backgrounds are estimated by extrapolation from a data control region in which the selection is identical to signal region except that the muon veto has been inverted (Fig. 2). In this muon control region, the W- and Z-boson contributions are measured by subtracting other sources of background, which are estimated using simulated samples. The extrapolation from the muon control region of the contribution in the muon-veto signal region is calculated using transfer factors as a function of m_{jet}. The transfer factors are measured in simulated samples of W- and Z-boson production in association with jets which are generated with SHERPA1.4.1 [36] with the CT10 [37] parton-distribution function (PDF) set. The Z-boson contribution is validated using data in a second control region with two muons and $E_{\mathrm{T}}^{\mathrm{miss}} > 350$ GeV, and the W-boson contribution is validated in a low-$E_{\mathrm{T}}^{\mathrm{miss}}$ control region with the same selection as signal region but $250 < E_{\mathrm{T}}^{\mathrm{miss}} < 350$ GeV.

Other sources of background are diboson production, top-quark pair production and single top production, which are estimated using simulated events. The MC@NLO generator [38] using the CT10

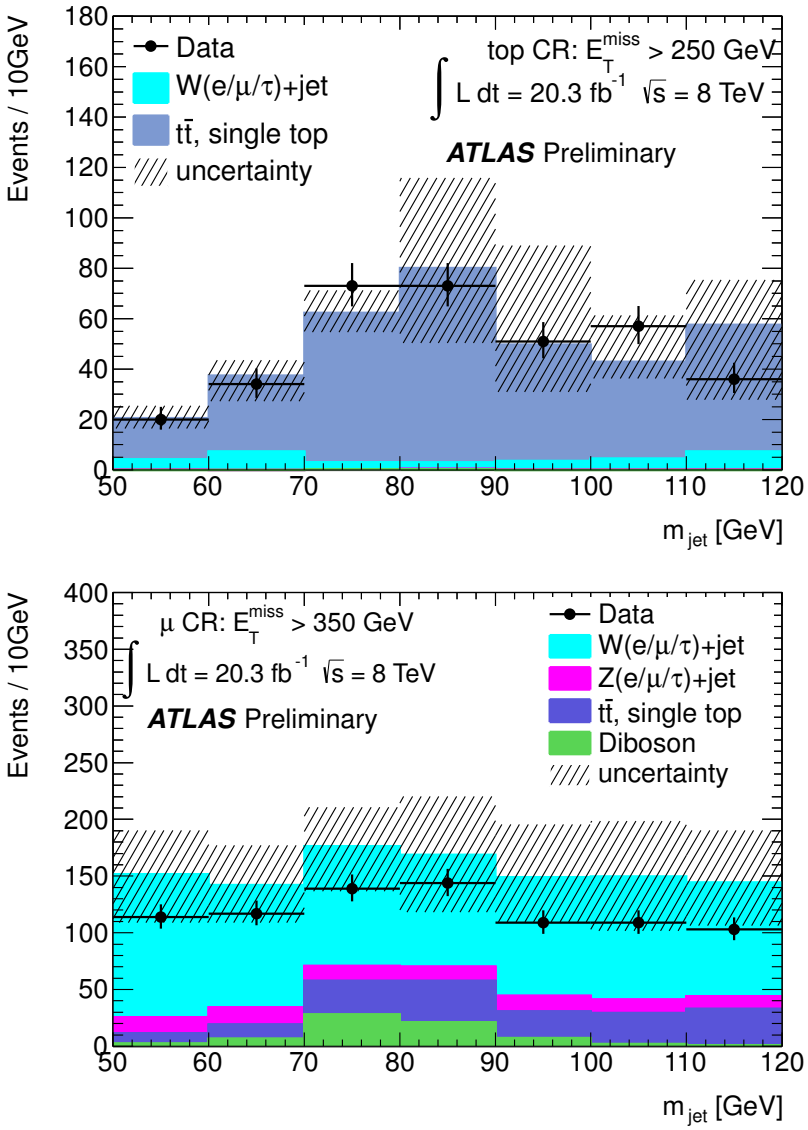

Figure 2: Data and predicted background in the control regions with one muon, one large-radius jet, two additional narrow jets and at least one b-tag and $E_{\mathrm{T}}^{\mathrm{miss}} > 250$ GeV (top) or one muon and $E_{\mathrm{T}}^{\mathrm{miss}} > 350$ GeV (bottom). Uncertainties include statistical and systematic sources.

PDF with the AUET2 [39] tune, interfaced to HERWIG6.520 [40] and JIMMY4.31 [41] for the simulation of underlying events, is used for the productions of $t\bar{t}$ and single-top processes, both s-channel and Wt production. The single-top t-channel process is generated with ACERMC3.8 [42] interfaced to PYTHIA8.1 [43], using the CTEQ6L1 [44] PDF with the AUET2B [39] tune. The diboson (ZZ, WZ and WW) samples are produced using the HERWIG6.520 generator with the CTEQ6L1 PDF and AUET2 [39] tune.

Background contributions from multi-jet production in which large $E_{\mathrm{T}}^{\mathrm{miss}}$ is due to mismeasured jet energies are estimated by extrapolating from a sample of events with two jets and found to be negligible [9].

Samples of simulated $pp \to W\chi\bar{\chi}$ and $pp \to Z\chi\bar{\chi}$ are generated using MADGRAPH5 [45], with showering and hadronization modeled by PYTHIA8.1 using AU2 [39] tune and CT10 PDF, including b-quarks in the initial state. Effective field theory operators (following the definitions of Ref. [20]) C1, D1, D5 and D9 are treated as representative of the full set of operators, where the D5 events are generated for both constructive ($C(u) = -C(d)$) and destructive ($C(u) = C(d)$) interference cases. In each case, $m_\chi = 1, 50, 100, 200, 400, 700, 1000$ and 1300 GeV are used.

The dominant sources of systematic uncertainty are due to the limited number of events in the control region, theoretical uncertainties in the simulated samples used for extrapolation, and uncertainties in the large-radius jet calibration and resolution [28]. Additional minor uncertainties are due to levels of initial-state and final-state radiation, parton distribution functions, lepton efficiency and momentum resolution.

The data and total predicted background in the two signal regions are shown in Table 1 and Fig. 3. The data agree well with the background estimate for both $E_{\mathrm{T}}^{\mathrm{miss}}$ thresholds. Exclusion limits at 90% confidence level (CL) are set on the dark matter signals using the predicted shape of the m_{jet} distribution and the CLs method [46], calculated with toy simulated experiments in which the systematic uncertainties have been integrated out. Fig. 4 shows the exlusion regions in the M_* vs m_χ plane for various operators.

Table 1: Data and estimated background yields in the two signal regions. Uncertainties include statistical and systematic contributions.

Process	$E_{\mathrm{T}}^{\mathrm{miss}} > 350$ GeV	$E_{\mathrm{T}}^{\mathrm{miss}} > 500$ GeV
$Z \to \nu\bar{\nu}$	400^{+39}_{-34}	54^{+8}_{-10}
$W \to \ell^{\pm}\nu$, $Z \to \ell^{\pm}\ell^{\mp}$	210^{+20}_{-18}	22^{+4}_{-5}
WW, WZ, ZZ	57^{+11}_{-8}	$9.1^{+1.3}_{-1.1}$
$t\bar{t}$, single t	39^{+10}_{-4}	$3.7^{+1.7}_{-1.3}$
Total	710^{+48}_{-38}	89^{+9}_{-12}
Data	705	89

Limits on the dark matter–nucleon scattering cross sections are reported using the method of Ref. [20] in Fig. 5 for both the spin-independent interaction model (C1, D1, D5) and the spin-dependent interaction model (D9). See Ref. [20] for discussion of the regions of validity of the effective field theory, which becomes a poor approximation if the mass of the intermediate particle M is below p_{T}^{W}. The results are compared with measurements from XENON100 [1], CDMS [2], CoGeNT [3], PICASSO [4], SIMPLE [5], IceCube [6] and COUPP [7]. This search for dark matter pair production in association with a W or Z boson extends the limits on the dark matter–nucleon scattering cross section in the low mass region $m_\chi < 10$ GeV where these direct detection experiments have less sensitivity. The new limits from this analysis are also compared to the limits set by ATLAS in the 7 TeV monojet analysis [9]. For the spin independent case the limits are improved by about three orders of magnitude for the case where the up-type and down-type couplings have opposite sign. For the other cases the limits are more similar.

In addition, limits are calculated on dark-matter $W\chi\bar{\chi}$ or $Z\chi\bar{\chi}$ production within two fiducial regions

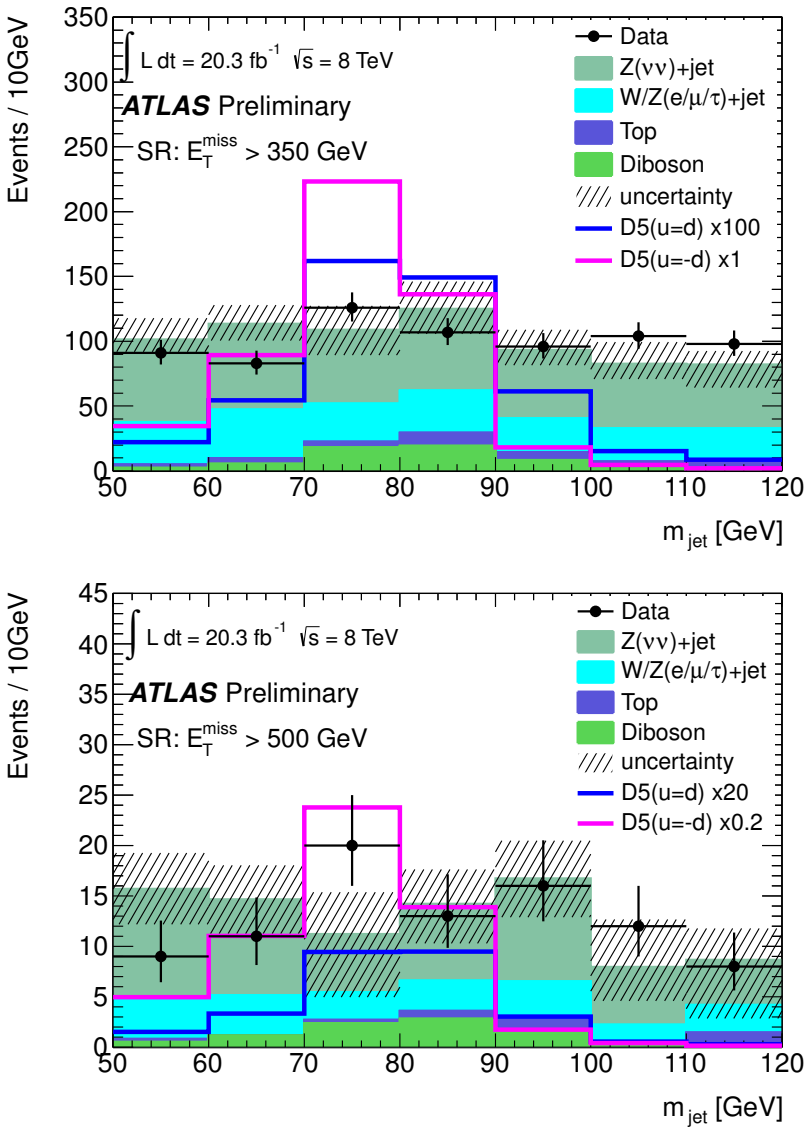

Figure 3: Data and predicted background in the signal region $E_{\mathrm{T}}^{\mathrm{miss}} > 350$ GeV and $E_{\mathrm{T}}^{\mathrm{miss}} > 500$ GeV. Combined single W/Z boson signal distributions of D5 destructive and D5 constructive case with dark matter mass of 1 GeV and $M_* = 1$ TeV are drawn as well. Uncertainties include statistical and systematic contributions.

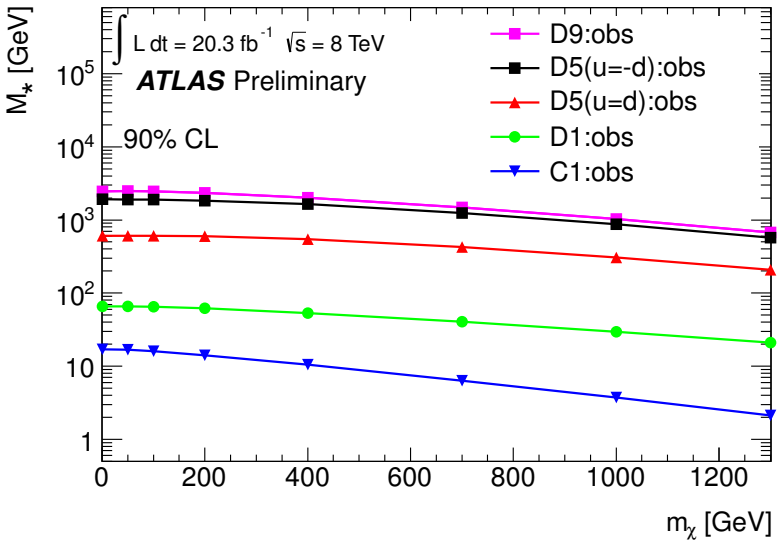

Figure 4: Summary of observed limits on the effective theory mass scale M_* at 90% CL for various operators from combined single W/Z boson signals. M_* values below these lines are excluded.

defined at parton level: $p_{\mathrm{T}}^{W\mathrm{or}Z} > 250$ GeV, $|\eta^{W\mathrm{or}Z}| < 1.2$, two quarks with $\sqrt{y} > 0.4$, $p_{\mathrm{T}}^{\chi\bar{\chi}} > 350$ or 500 GeV. The upper limit on cross section times reconstruction efficiency is 3 fb (1.5 fb) at 95% C.L. for $p_{\mathrm{T}}^{\chi\bar{\chi}} > 350$ (500 GeV). The reconstruction efficiency for these events is $50 \pm 1\%$, with modest dependence on the dark-matter production model.

In conclusion, this paper reports the first LHC limits on dark-matter production in events with a hadronically decaying W or Z boson and large missing transverse momentum. In the case of constructive intereference between up-type and down-type contributions, the results set the strongest limits on the mass scale of M_* of the unknown mediating interaction.

References

[1] XENON100 Collaboration Collaboration, E. Aprile et al., Phys. Rev. Lett. **109** (2012) 181301, arXiv:1207.5988 [astro-ph.CO].

[2] CDMS Collaboration Collaboration, Z. Ahmed et al., Phys. Rev. Lett. **106** (2011) 131302, arXiv:1011.2482 [astro-ph.CO].

[3] CoGeNT Collaboration Collaboration, C. Aalseth et al., Phys. Rev. Lett. **106** (2011) 131301, arXiv:1002.4703 [astro-ph.CO].

[4] PICASSO Collaboration Collaboration, S. Archambault et al., Phys. Lett. B **711** (2012) 153–161, arXiv:1202.1240 [hep-ex].

[5] M. Felizardo et al., Phys. Rev. Lett. **108** (2012) 201302, arXiv:1106.3014 [astro-ph.CO].

[6] IceCube collaboration Collaboration, M. Aartsen et al., Phys. Rev. Lett. **110** (2013) 131302, arXiv:1212.4097 [astro-ph.HE].

[7] COUPP Collaboration Collaboration, E. Behnke et al., Phys. Rev. Lett. **106** (2011) 021303, arXiv:1008.3518 [astro-ph.CO].

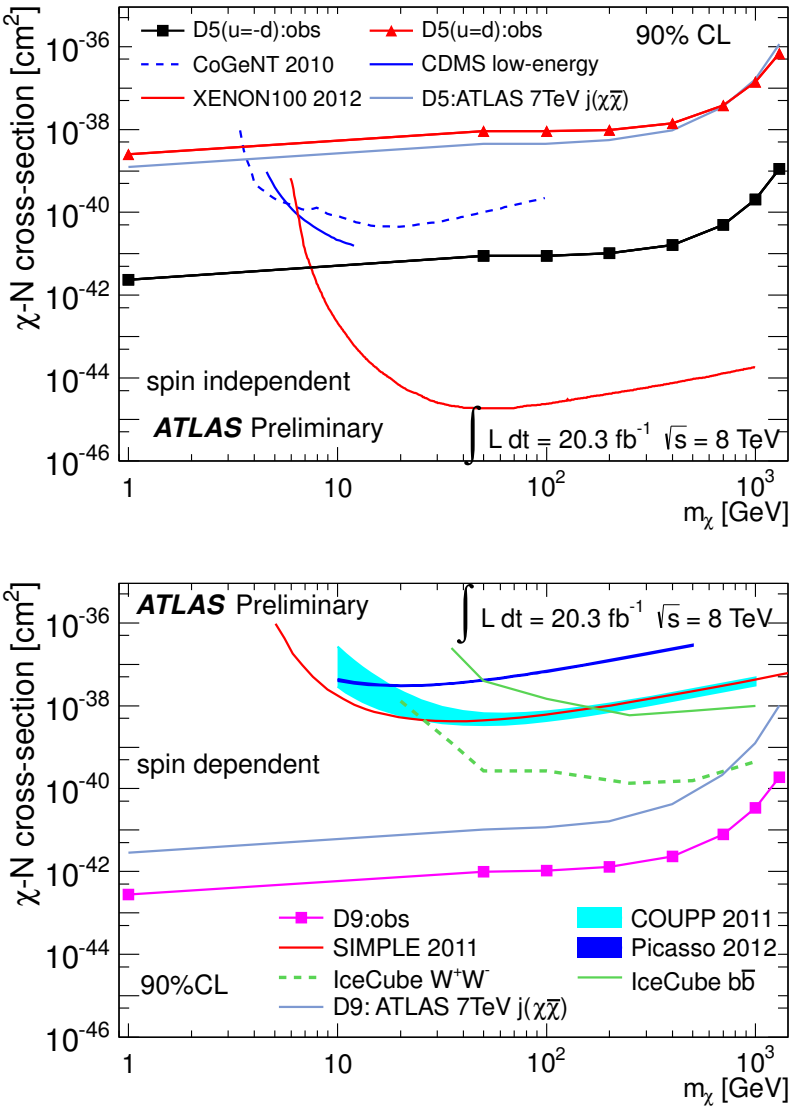

Figure 5: Limits on χ-nucleon cross sections, compared to previous limits set by direct dark matter detection experiments [1, 2, 3, 4, 5, 6, 7] and by the ATLAS 7 TeV monojet analysis [9]. The top plot shows the limits for spin-independent scattering and the bottom plot shows them for spin-dependent scattering. All limits are shown at 90% CL.

[8] CDF Collaboration Collaboration, T. Aaltonen et al., Phys. Rev. Lett. **108** (2012) 211804, arXiv:1203.0742 [hep-ex].

[9] ATLAS Collaboration, JHEP **04** (2013) 075, arXiv:1210.4491 [hep-ex].

[10] CMS Collaboration, JHEP **09** (2012) 094, arXiv:1206.5663 [hep-ex].

[11] ATLAS Collaboration, Phys. Rev. Lett. **110** (2013) 011802, arXiv:1209.4625 [hep-ex].

[12] CMS Collaboration, Phys. Rev. Lett. **108** (2012) 261803, arXiv:1204.0821 [hep-ex].

[13] Y. Bai and T. M. Tait, Phys. Lett. B **723** (2013) 384–387, arXiv:1208.4361 [hep-ph].

[14] ATLAS Collaboration, JHEP **03** (2013) 128, arXiv:1211.6096 [hep-ex].

[15] L. M. Carpenter, A. Nelson, C. Shimmin, T. M. Tait, and D. Whiteson, Phys. Rev. D **87** (2013) 074005, arXiv:1212.3352 [hep-ex].

[16] Q. Cao, C. Chen, C. Li, and H. Zhang, JHEP **08** (2011) 018, arXiv:0912.4511 [hep-ph].

[17] M. Beltran, D. Hooper, E. Kolb, Z. Krusberge, and T. Tait, JHEP **08** (2011) 018, arXiv:1002.4137 [hep-ph].

[18] J. Goodman, M. Ibe, A. Rajaraman, W. Shepherd, T. Tait, and H. Yu, Phys. Lett. B **695** (2011) 185, arXiv:1005.1286 [hep-ph].

[19] Y. Bai, P. Fox, and R. Harnik, JHEP **12** (2010) 048, arXiv:1005.3797 [hep-ph].

[20] J. Goodman, M. Ibe, A. Rajaraman, W. Shepherd, T. Tait, and H. Yu, Phys. Rev. D **82** (2010) 116010, arXiv:1008.1783 [hep-ph].

[21] A. Rajaraman, W. Shepherd, T. Tait, and A. Wijangco, Phys. Rev. D **84** (2011) 095013, arXiv:1108.1196 [hep-ph].

[22] P. Fox, R. Harnik, J. Kopp, and Y. Tsai, Phys. Rev. D **85** (2012) 056011, arXiv:1109.4398 [hep-ph].

[23] K. Cheung, P. Tseng, Y. Tsai, and T. Yuan, JCAP **1205** (2012) 001, arXiv:1201.3402 [hep-ph].

[24] R. Cotta, J. Hewett, M. Le, and T. Rizzo, (2012) , arXiv:1210.0525 [hep-ph].

[25] ATLAS Collaboration, JINST **3** (2008) S08003.

[26] ATLAS Collaboration, submitted to Eur. Phys. J. C (2013), arXiv:1302.4393 [hep-ex].

[27] Y. Dokshitzer, G. Leder, S. Moretti, and B. Webber, JHEP **08** (1997) 001, arXiv:hep-ph/9707323.

[28] ATLAS Collaboration, submitted to JHEP (2013), arXiv:1306.4945 [hep-ex].

[29] J. M. Butterworth, A. R. Davison, M. Rubin, and G. P. Salam, Phys. Rev. Lett. **100** (2008) 242001, arXiv:0802.2470 [hep-ph].

[30] M. Cacciari, G. P. Salam, and G. Soyez, JHEP **04** (2008) 063, arXiv:0802.1189 [hep-ph].

[31] ATLAS Collaboration, ATL-LARG-PUB-2009-001-2. https://cds.cern.ch/record/1112035.

[32] ATLAS Collaboration, Eur. Phys. J. C **72** (2012) 1909, arXiv:1110.3174 [hep-ex].

[33] ATLAS Collaboration, ATLAS-CONF-2011-063. https://cdsweb.cern.ch/record/1345743.

[34] ATLAS Collaboration, Eur. Phys. J. C **73** (2013) 2304, arXiv:1112.6426 [hep-ex].

[35] ATLAS Collaboration, Eur. Phys. J. C **72** (2012) 1844, arXiv:1108.5602 [hep-ex].

[36] T. Gleisberg, S. Hoeche, F. Krauss, M. Schoenherr, S. Schumann, F. Siegert, and J. Winter, JHEP **02** (2009) 007, arXiv:0811.4622 [hep-ph].

[37] H. Lai, M. Guzzi, J. Huston, Z. Li, P. Nadolsky, J. Pumplin, and C. Yuan, Phys. Rev. D **82** (2010) 074024, arXiv:1007.2241 [hep-ph].

[38] S. Frixione and B. R. Webber, JHEP **06** (2002) 029, arXiv:hep-ph/0204244.

[39] ATLAS Collaboration, ATL-PHYS-PUB-2011-008. https://cds.cern.ch/record/1345343.

[40] G. Corcella, I. G. Knowles, G. Marchesini, S. Moretti, K. Odagiri, P. Richardson, M. H. Seymour, and B. R. Webber, JHEP **01** (2001) 010, arXiv:hep-ph/0011363.

[41] J. Butterworth, J. Forshaw, and M. Seymour, Z. Phys. C **72** (1996) 637–646, arXiv:hep-ph/9601371.

[42] B. P. Kersevan and E. Richter-Was, Comput. Phys. Commun. **184** (2013) 919–985, arXiv:hep-ph/0405247.

[43] T. Sjostrand, S. Mrenna, and P. Z. Skands, Comput. Phys. Commun. **178** (2008) 852–867, arXiv:0710.3820 [hep-ph].

[44] J. Pumplin et al., JHEP **07** (2002) 012, arXiv:hep-ph/0201195.

[45] J. Alwall, M. Herquet, F. Maltoni, O. Mattelaer, and T. Stelzer, JHEP **06** (2011) 128, arXiv:1106.0522 [hep-ph].

[46] A. L. Read, J. Phys. G **28** (2002) 2693–2704.

Additional Plots

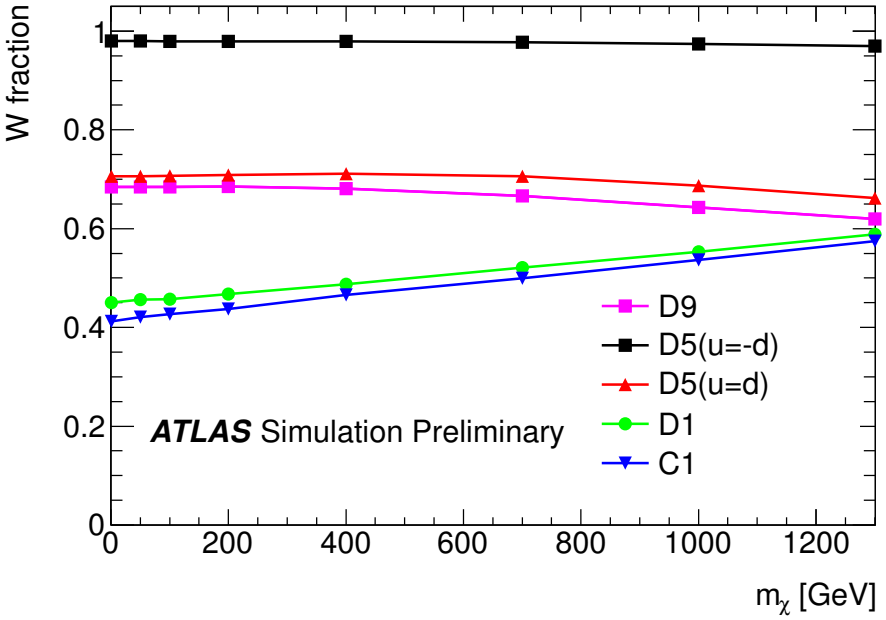

Figure 6: Fraction of W bosons in combined single W/Z-boson signal samples at different dark matter masses.

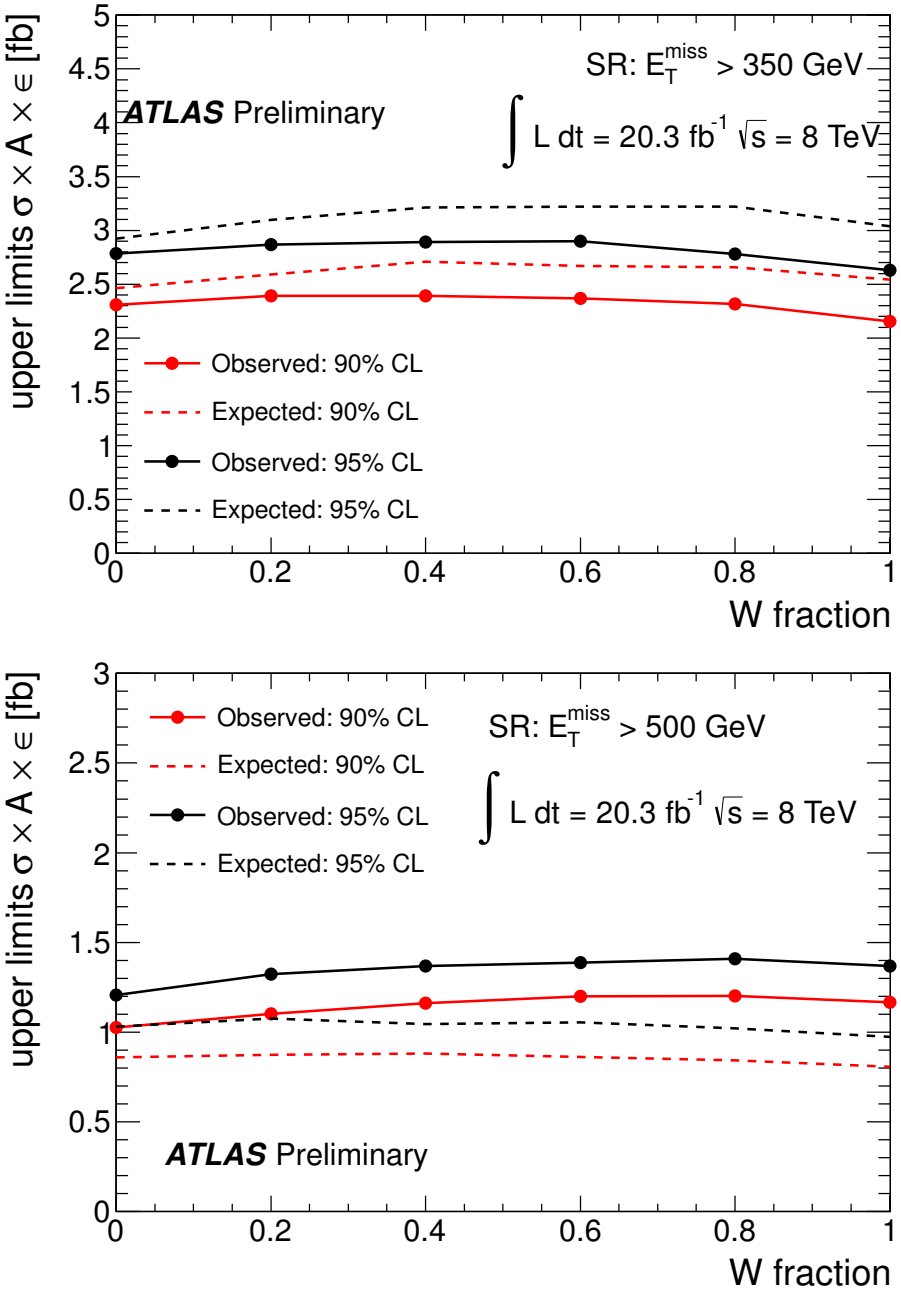

Figure 7: Limits on $\sigma \times A \times \epsilon$ as a function of W-boson fraction in combined single W/Z-boson signal samples, derived from taking W- and Z-boson peaks in D5 destructive operator $m_\chi = 1$ GeV. Top: limits from signal region (SR) $E_{\mathrm{T}}^{\mathrm{miss}} > 350$ GeV. Bottom: limits from SR $E_{\mathrm{T}}^{\mathrm{miss}} > 500$ GeV.

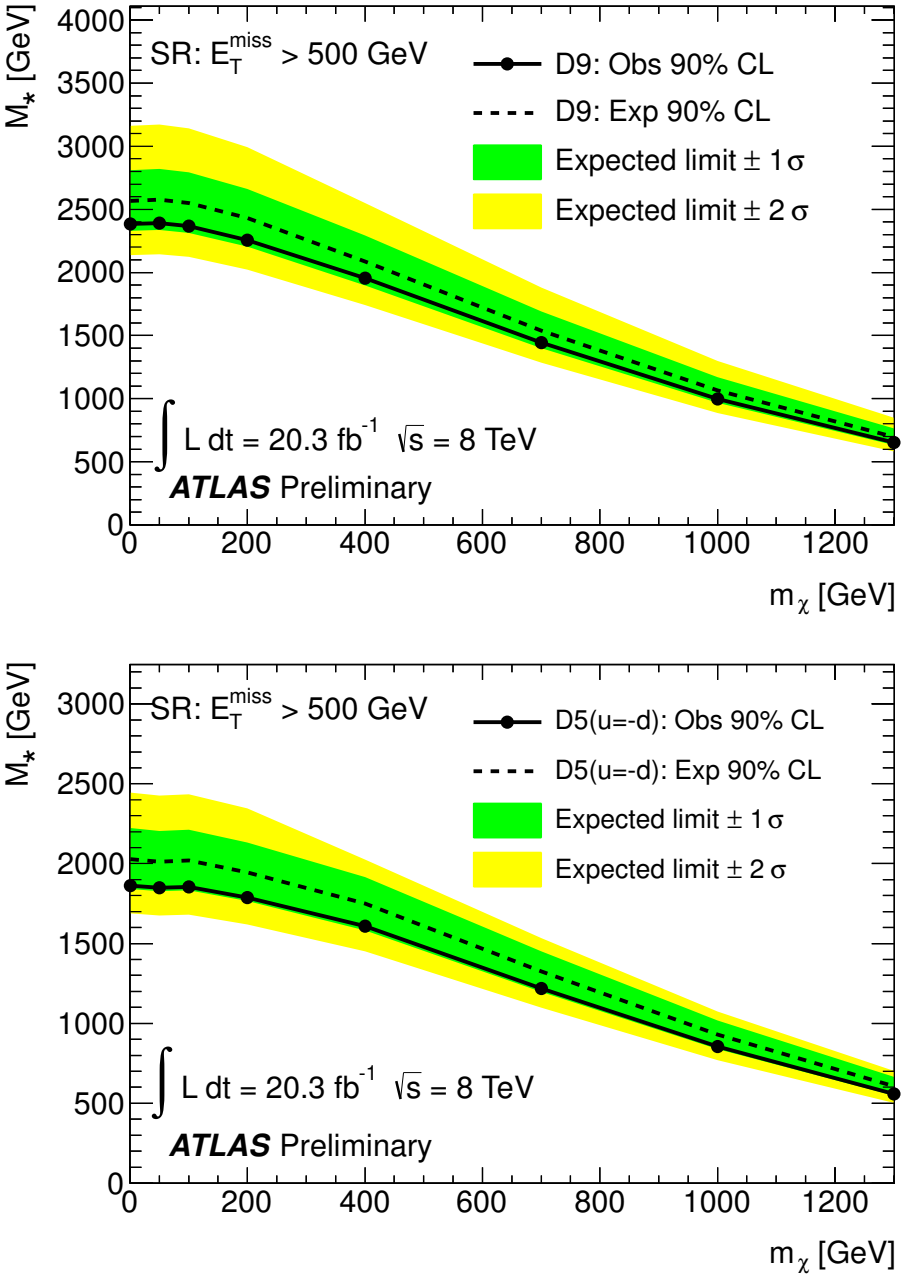

Figure 8: 90% CL M_* limits for D9 and D5 constructive operators from combined mono-W-boson and mono-Z-boson signals from SR $E_{\mathrm{T}}^{\mathrm{miss}} > 500$ GeV.

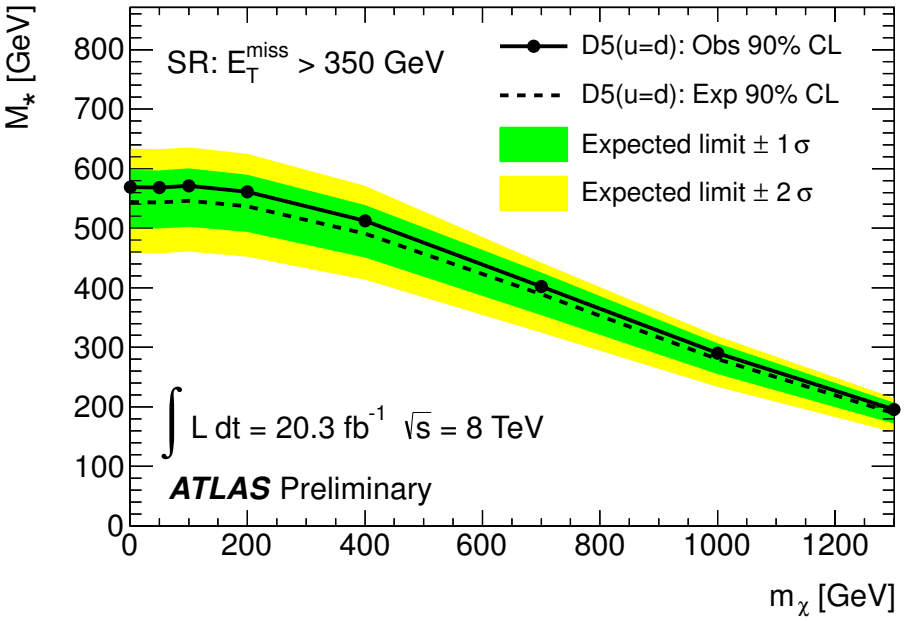

Figure 9: 90% CL M_* limits for D5 destructive operators from combined mono-W-boson and mono-Z-boson signals from SR $E_{\mathrm{T}}^{\mathrm{miss}} > 350$ GeV.

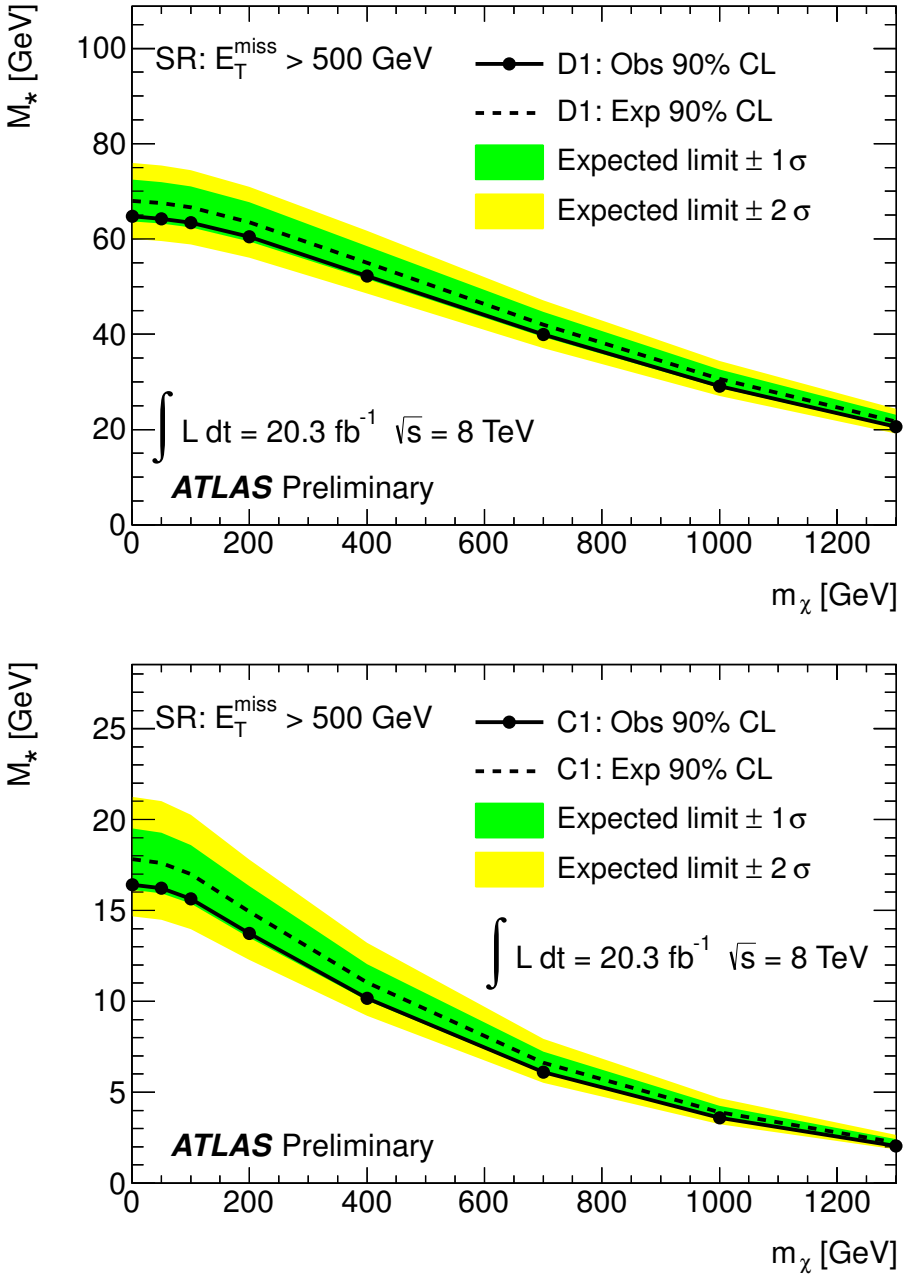

Figure 10: 90% CL M_* limits for D1 and C1 operators from combined mono-W-boson and mono-Z-boson signals from SR $E_{\mathrm{T}}^{\mathrm{miss}} > 500$ GeV.

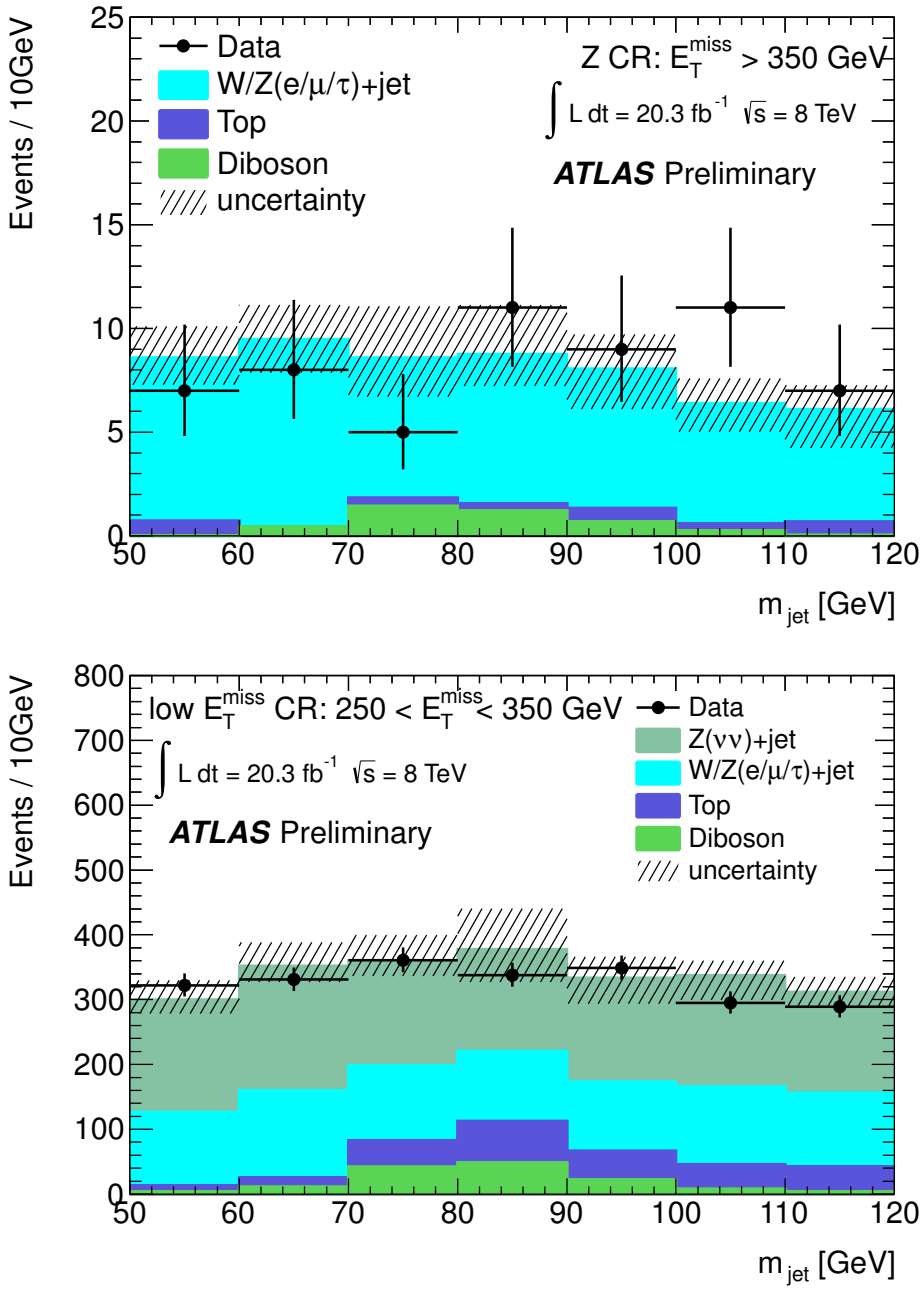

Figure 11: Reconstructed jet mass in $Z(\mu\mu)$ control region with $E_{\mathrm{T}}^{\mathrm{miss}} > 350$ GeV and low-$E_{\mathrm{T}}^{\mathrm{miss}}$ control region with $E_{\mathrm{T}}^{\mathrm{miss}} \in [250, 350]$ GeV.